Chinese Chemical Letters 32 (2021) 3553–3557

Contents lists available at ScienceDirect

Chinese Chemical Letters

journal homepage: www.elsevier.com/locate/cclet

Communication

Enriching redox active sites by interconnected nanowalls-like nickel cobalt phospho-sulfide nanosheets for high performance supercapacitors

Kaiyang Zhang[a,1], Yazhou Xu[a,1], Yingchun Lin[a,1], Yushuai Xiong[a], Jun Huang[a], Li Wang[a], Mengke Peng[a], Ting Hu[b], Kai Yuan[a,*], Yiwang Chen[a,c,**]

[a] Institute of Polymers and Energy Chemistry (IPEC), College of Chemistry, Nanchang University, Nanchang 330031, China
[b] School of Materials Science and Engineering, Nanchang University, Nanchang 330031, China
[c] Institute of Advanced Scientific Research (iASR), Jiangxi Normal University, Nanchang 330022, China

ARTICLE INFO

Article history:
Received 27 January 2021
Received in revised form 10 February 2021
Accepted 17 February 2021
Available online 19 February 2021

Keywords:
Nickel cobalt phospho-sulfide
Electrodeposition
Specific capacitance
Asymmetric supercapacitors
Energy density

ABSTRACT

Although transition metal phospho-sulfides deliver outstanding electrochemical performance, complex preparation methods hindered their further development. Herein, we report a facile one-step electrodeposition approach to deposit interconnected nanowalls-like nickel cobalt phospho-sulfide (Ni-Co-P-S) nanosheets onto the surface of carbon cloth. The thin Ni-Co-P-S nanosheets with multi-components and synergetic effects delivered rich active sites, further enhancing reversible capacitance. Therefore, the as-prepared Ni-Co-P-S electrode materials exhibit excellent electrochemical performance in a three-electrode system, showcasing a high specific capacitance of 2744 F/g at 4 A/g. The full supercapacitors based on Ni-Co-P-S as positive electrode and active carbon as negative electrode showcase a high specific capacitance of 110.9 F/g at 1 A/g, impressive energy density of 39.4 Wh/kg at a power density of 797.5 W/kg in terms of excellent cycling stability (91.87% retention after 10,000 cycles). This simple electrode position strategy for synthesizing Ni-Co-P-S can be extended to prepare electrode materials for various sustainable electrochemical energy storage/conversion technologies.

Recently, the powerful and efficient energy storage and conversion has become one of the primary efforts of scientific research [1–3]. Transition metal sulfides (TMSs) have been extensively researched as promising materials for energy storage and conversion, such as zinc/sodium-ion batteries [4,5], supercapacitors (SCs) [6,7], Zn-air batteries [8,9] and water splitting [10,11]. Especially, SCs have attracted continuous attention for the high power density, cycling durability and safety [12]. TMSs have been extensively studied as electrode materials for SCs because they can improve the energy density of SCs by their relatively superb specific capacitance generated from multiple oxidation states of transition metal [13].

Due to the lack of sufficient redox reaction activity and relatively poor electronic conductivity, the electrochemical performance of mono-metal sulfides such as cobalt sulfide, nickel sulfide, tungsten sulfide and molybdenum sulfide are unsatisfactory in many cases [14]. Mixed metal sulfides possess higher electronic conductivity and more abundant redox active sites in contrast to the mono-metal sulfides, leading to significant augmentation of electrochemical performances [15,16]. Especially, nickel cobalt sulfides can be used as decent positive electrode materials for various types of electrochemical energy storage, because of their ultrahigh theoretical capacitance [17–19]. However, the electrochemical performances of TMSs are still far from outstanding, of which the rate capability and ion diff ;usion kinetics are usually poor and sluggish owing to the low electrical conductivity, severely retarding their further development [20,21].

Heterogeneous nanostructure, which is comprised of multiple components, has been devoted to enhance the intrinsic electrical conductivity of TMSs, exhibiting synergistically enhanced activity [22,23]. Besides, rational structure design could fulfill promotive function by synergistic effects between each component in the heterogeneous nanostructure. A myriad of redox active sites, fast electron transfer, and ion diffusion/transport can be effectively achieved [24]. Therefore, the preparation of supercapacitor

* Corresponding author.
** Corresponding author at: Institute of Polymers and Energy Chemistry (IPEC), College of Chemistry, Nanchang University, Nanchang 330031, China.
E-mail addresses: kai.yuan@ncu.edu.cn (K. Yuan), ywchen@ncu.edu.cn (Y. Chen).
[1] These authors contributed equally to this work.

https://doi.org/10.1016/j.cclet.2021.02.034

materials with heterogeneous nanostructure is a problem-solving strategy to improve its electrochemical performance. More recently, many efforts have demonstrated to optimize the electrochemical properties of TMSs by substituting sulfur with phosphorus heteroatom. For instance, Jiang *et al.* have presented a facile anionic P substitution approach to prepare nickel phospho-sulfide nanoparticles on graphene nanosheets (G/Ni-S-P) for SCs. The synergistic eff ;ects between each component as well as hierarchical structure have positive effects on energy storage, leading to the resultant G/Ni-S-P electrode possesses an excellent specific capacitance of 1406 C/g at 1 A/g and a rate capability of 60.2% at 120 A/g [25]. Lei *et al.* have synthesized phospho-sulfide (Zn-Ni-P-S) nanosheets grown on Ni foam by a two-step strategy, which combines a hydrothermal approach with a phosphorization and sulfurization process. The Zn-Ni-P-S delivered a high specific capacitance of 1180 C/g at 2 A/g [26]. Nevertheless, the recipes mentioned above involve multistep processes which lead to the application of the transition metallic phospho-sulfides costly, complicated, and time-consuming, although the prepared materials have excellent electrochemical performance.

Compared to other synthesis strategies such as ball-milling and hydrothermal method, electrochemical deposition has their unique advantages as follow. In the first place, this technology has a wide range of applications. It can be used to prepare many electrode materials, including conductive polymers, metal oxides, metal sulfides, and so on. In addition, the strategy can work under extremely mild conditions using simple experimental devices (electrochemical workstation and electrolyzer) [27]. Most importantly, active electrochemical materials with different morphologies and properties can be easily prepared by adjusting the reaction conditions (reaction temperature, concentration, time, *etc.*) [28]. Therefore, a great number of works have been done to prepare materials by electrochemical deposition. However, the preparation of TMPS materials *via* one-step electrodeposition is rarely reported, and still a challenge.

In light of the above considerations, herein, a facile one-step electrodeposition synthesis has been designed to deposit nickel cobalt phospho-sulfide (Ni-Co-P-S) nanosheets onto the surface of carbon cloth (CC). Due to the outstanding conductivity of the CC substrate as well as the synergistic effect of multiple components, the obtained Ni-Co-P-S electrode with enriched redox active sites delivered an outstanding specific capacitance of 2744 F/g at 4 A/g and decent rate capability. Furthermore, an asymmetric supercapacitor was fabricated with Ni-Co-P-S as the positive electrode and active carbon as the negative electrode, achieving an excellent energy density of 39.4 Wh/kg at a power density of 797.5 W/kg with superior electrochemical cycling stability (91.87% retention after 10,000 cycles).

The preparation of nickel cobalt phospho-sulfide (Ni-Co-P-S) on carbon cloth (CC) is illustrated in Fig. 1a. The Ni-Co-P-S nanosheets were deposited onto CC by a facile one-step electrodeposition synthesis under room temperature. Apparently, as demonstrated by the scanning electron microscope (SEM) images (Figs. 1b and c), the nanowalls-like Ni-Co-P-S nanosheets are homogeneously aligned on CC. In addition, the morphologies of Ni-Co-S (prepared without $NaH_2PO_2{\cdot}H_2O$) and Ni-Co-P (prepared without CH_4N_2S) were shown in Figs. S1 and S2 (Supporting information), respectively, which also reveal that interconnected nanosheets are aligned on the fiber surfaces. The well-defined nanowalls-like structures on the CC substrate is conducive to fast ions transportation.

To further investigate the nanostructure of as-prepared Ni-Co-P-S, the Ni-Co-P-S-2 layer was peeled off from the CC substrate by strong ultrasonication and used for transmission electron microscopy (TEM) observation. Figs. 1d and e exhibit typical TEM images of a piece of Ni-Co-P-S-2, from which many nanosheets vertically aligned onto a film could be observed. As observed from the high resolution TEM (HRTEM) image shown in Fig. 1f, the interplanar spacings of 0.222 and 0.260 nm are corresponded to the (210) plane of Ni_5P_4 and (311) plane of $NiCo_2S_4$, respectively. Moreover, energy-dispersive X-ray spectrometry (EDS) elemental mapping images of Co, Ni, P and S for the Ni-Co-P-S-2 sample, using an SEM, are presented in Fig. 1g. Excellent coverage and uniform distribution of these elements indicate that Ni-Co-P-S-2 grows well on CC. EDS elemental mapping images of Ni-Co-S (Fig. S3 in Supporting information) and Ni-Co-P (Fig. S4 in Supporting

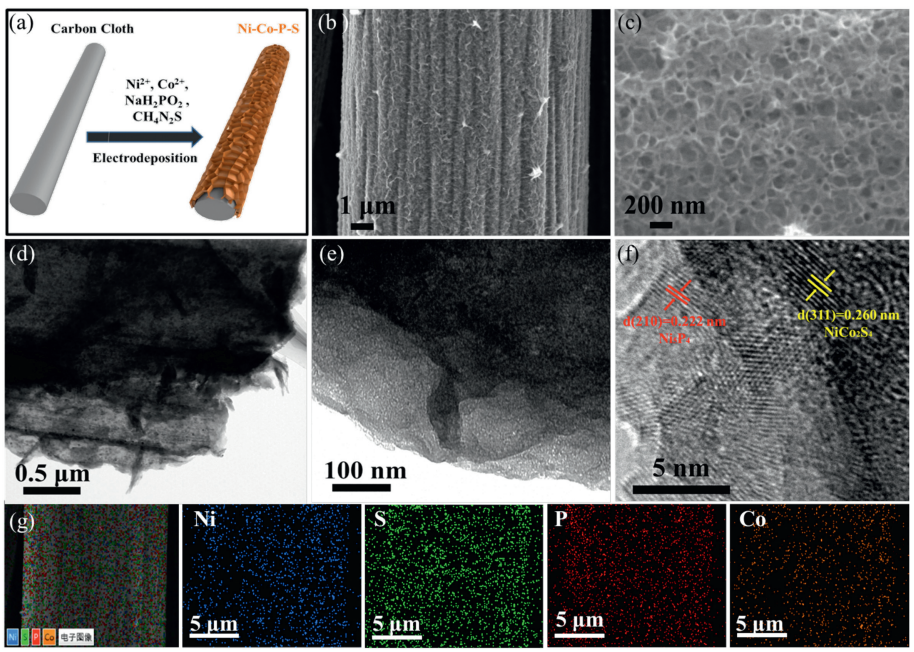

Fig. 1. (a) Schematic representation of the preparation of Ni-Co-P-S on CC. (b, c) SEM images, (d, e) TEM images, (f) HRTEM image and (g) corresponding elemental mapping images of Ni-Co-P-S-2.

information) demonstrated the homogeneous distribution of all the elements, suggesting the successful preparation of the materials.

XRD can be used to testify the phase compositions of the as-prepared samples. One sharp peak derived from carbon cloth was shown in the XRD patterns of the Ni-Co-P-S-2 (Fig. 2a), Ni-Co-S (Fig. S5a in Supporting information) and Ni-Co-P (Fig. S5b in Supporting information). In Fig. 2a, the characteristic peak signals of Ni_5P_4 (JCPDS No. 18-0883) and $NiCo_2S_4$ (JCPDS No. 20-0782) phases were observed in the XRD pattern of the Ni-Co-P-S-2, demonstrating the presence of Ni_5P_4 and $NiCo_2S_4$ phases after the electrodeposition process [29,30].

The elemental compositions and the chemical valence states of the surface atoms for the Ni-Co-P-S-2 were examined by XPS. The XPS survey spectrum of Ni-Co-P-S-2 suggests the existence of Co, Ni, P, and S elements (Fig. 2b). The surface atomic ratios in Ni-Co-P-S-2 are 21.02% (Co), 32.77% (Ni), 30.27% (P) and 14.05% (S), respectively. The XPS spectra of Ni 2p and Co 2p in Figs. 2c and d can be deconvoluted into two spin-orbiting dipoles and two shakeup satellites (labeled as "Sat."). As showcased in Fig. 2c, the peaks centered at binding energies of 857.8 eV and 875.6 eV are ascribed to the Ni^{3+}, and 856.8 eV and 873.6 eV are ascribed to the Ni^{2+} [31]. Meanwhile, in Fig. 2d, the fitting peaks centered at binding energies of 781.3 eV and 797.0 eV can be ascribed to the Co^{3+}, and 783.3 eV and 799.0 eV are corresponded to the Co^{2+} [32]. In the high-resolution spectra of P 2p (Fig. 2e), the peaks centered at 135.5 eV and 134.5 eV are characteristic of P $2p_{3/2}$ and P $2p_{1/2}$, respectively [33]. For S 2p (Fig. 2f), the peaks located at 163.1 eV and 164.8 eV are characteristic of S $2p_{3/2}$ and S $2p_{1/2}$, respectively, which are associated with metal-sulfur bonds [34]. These results further proved that metal phospho-sulfides were successfully prepared. The surface information of Ni-Co-S and Ni-Co-P was also demonstrated by XPS spectra (Figs. S6 and S7 in Supporting information). The high resolution XPS spectra of Ni 2p, Co 2p, S 2p and P 2p spectra also suggested the two control samples were successfully fabricated.

To evaluate the electrochemical performance of the as-prepared electrodes, cyclic voltammetry (CV), electrochemical impedance spectroscopy (EIS), and galvanostatic charge/discharge (GCD) tests were implemented. Firstly, the influence of the thiourea contents on electrochemical performance during electrodepositing Ni-Co-P-S were studied. Four different bimetallic phospho-sulfides with different contents of sulfur (named as Ni-Co-P-S-1 to Ni-Co-P-S-4), have been investigated (see Experimental Section in Supporting information for detail). The CV curves of Ni-Co-P-S samples with different sulfur contents at the scan rate of 10 mV/s were displayed in Fig. S8a (Supporting information). The integrated CV area of Ni-Co-P-S-2 is obviously larger than those for Ni-Co-P-S-1, Ni-Co-P-S-3 and Ni-Co-P-S-4, which proves that Ni-Co-P-S-2 shows the largest specific capacitance. The GCD measurements of Ni-Co-P-Ss were implemented in 0–0.45 V at 5 A/g (Fig. S8b in Supporting information). Based on the GCD profiles, the specific capacitances of Ni-Co-P-S-1 to Ni-Co-P-S-4 are 983, 2744, 1958 and 1289 F/g, respectively. Obviously, the result that Ni-Co-P-S-2 has the largest specific capacitance obtained from GCD is consistent with that of CV. Besides, the Ni-Co-P-S-2 shows the best conductivity among all the Ni-Co-P-S samples, as demonstrated by EIS in Fig. S8c (Supporting information).

For further investigating the synergistic advantages of phosphorus and sulfur, the electrochemical performances of Ni-Co-S and Ni-Co-P were reviewed for comparison. The CV curves of Ni-Co-P-S-2, Ni-Co-S and Ni-Co-P electrodes at 10 mV/s within 0–0.45 V are showcased in Fig. 3a. The CV curves of the above electrodes reveal the faradaic redox reaction behavior of each electrode, which is proved by a pair of redox peaks. The integrated CV area of Ni-Co-P-S-2 is obviously larger than Ni-Co-P and Ni-Co-S, which proves that Ni-Co-P-S-2 delivers a larger specific capacitance. In addition, the CV curves are totally different when the S content is different. The electronegativity of S is relatively higher than that of P, leading to the trend of Ni and Co oxidation for Ni-Co-S is harder. Therefore, the oxidation peak of Ni-Co-S (0.36 V) is higher than those of Ni-Co-P (0.20 V) and Ni-Co-P-S-2 (0.25 V). The CV curves of Ni-Co-P-S-2 varies from 5 mV/s to 60 mV/s in a voltage range of 0–0.45 V (Fig. S9 in Supporting information) apparently shows pseudocapacitive characteristics, owing to their significant difference from an ideal rectangular shape. Furthermore, GCD curves for Ni-Co-P-S-2, Ni-Co-S and Ni-Co-P electrodes in the potential range of 0–0.45 V were recorded at a fixed current density of 5 A/g. The observed non-linear shape for all GCD curves again confirmed faradaic dominant electrochemical reactions within the electrodes. It was clear that the discharge time for Ni-Co-P-S-2 is longer than Ni-Co-S and Ni-Co-P, suggesting the highest specific capacitance, which is consistent with the CV results (Fig. 3b). The GCD measurements of Ni-Co-P-S-2 (Fig. S10 in Supporting information), Ni-Co-S (Fig. S11 in Supporting information) and Ni-Co-P (Fig. S12 in Supporting information) electrodes were implemented in the voltage window of 0–4.5 V at different current densities (Fig. 3c). The specific gravimetric capacitances of Ni-Co-P-S-2 are 2744, 2733, 2712, 2695, 2635, 2580, 2477, 1446, 2382 and 2288 F/g at 4, 5, 8, 10, 20, 30, 50, 60, 80 and 100 A/g,

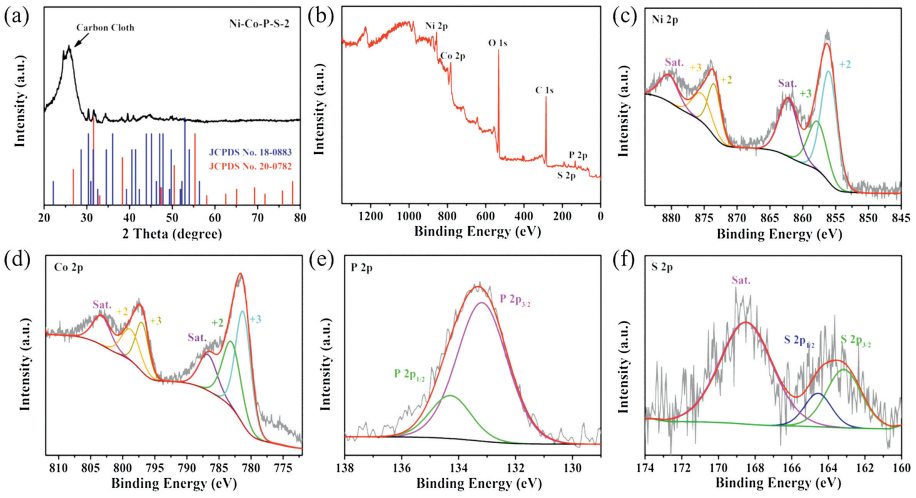

Fig. 2. (a) XRD pattern of Ni-Co-P-S-2. (b) XPS survey scan spectrum of Ni-Co-P-S-2. High resolution XPS spectra of (c) Ni 2p, (d) Co 2p, (e) P 2p and (f) S 2p.

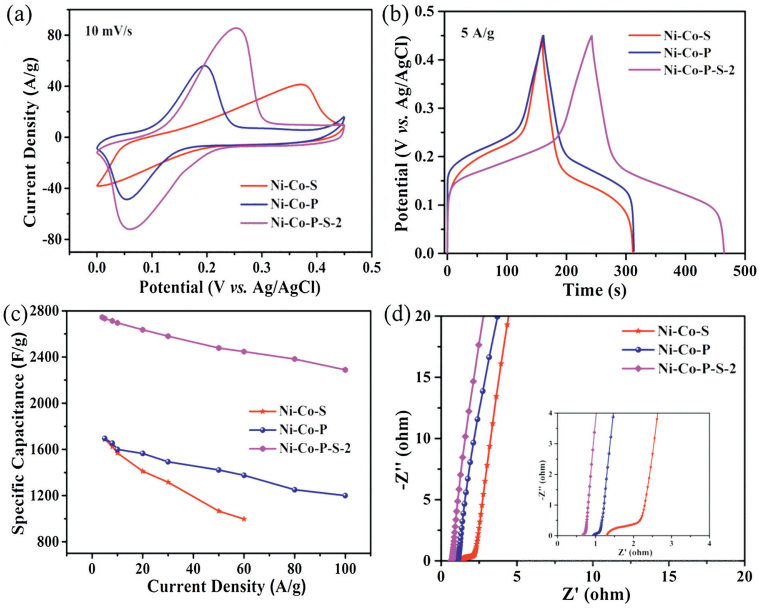

Fig. 3. (a) CV curves of Ni-Co-S, Ni-Co-P and Ni-Co-P-S-2 at 10 mV/s. (b) GCD curves of Ni-Co-S, Ni-Co-P and Ni-Co-P-S-2 at 5 A/g. (c) Specific capacitances of Ni-Co-S, Ni-Co-P and Ni-Co-P-S-2 at different current densities. (d) EIS curves of Ni-Co-S, Ni-Co-P and Ni-Co-P-S-2 (The inset is the partial enlarged Nyquist plots).

respectively, suggesting the high specific capacitances and rate capacity (only drops by 16.62% when the current density rises from 4 A/g to 100 A/g). The reason for the good electrochemical performance of Ni-Co-P-S-2 is that the mixed valence Ni, Co, P and S atoms are benefit for the formation of ionic and electronic defects, which can act as active sites for Faraday reaction.

To better understand the influence of the synergistic effect of phosphorus and sulfur, the electrochemical impedances of Ni-Co-P-S-2, Ni-Co-S and Ni-Co-P were tested by using EIS (Fig. 3d). In the high-frequency region, Ni-Co-P-S-2 displays a smaller semicircle diameter than Ni-Co-P and Ni-Co-S because of a lower charge-transfer impedance. At the same time, the Ni-Co-P-S-2 possesses the equivalent series resistance of 0.73 Ω, that is lower than 1.14 Ω for Ni-Co-P and 2.21 Ω for Ni-Co-S. In the low-frequency region, the slope of Ni-Co-P-S-2 showcases the lowest diffusion resistance. The EIS results demonstrate that the

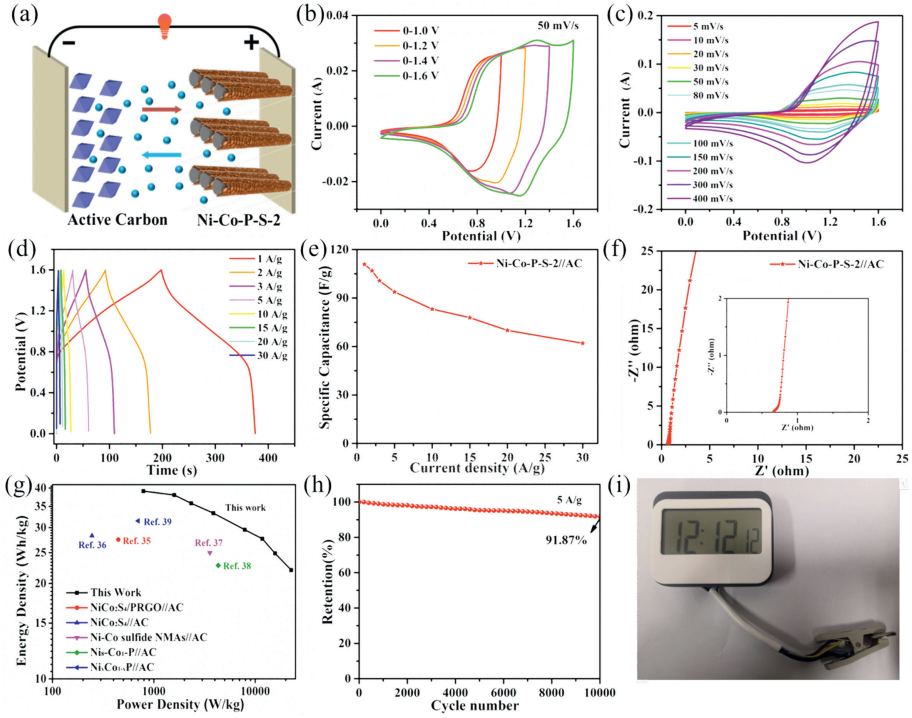

Fig. 4. (a) Schematic representation of Ni-Co-P-S-2//AC device. (b) CV curves under various potential windows at 50 mV/s. (c) CV curves at different scan rates. (d) GCD curves and (e) specific capacitances at different current densities. (f) EIS curve (the inset is the partial enlarged Nyquist plots). (g) Ragone plots of energy density and power density compared with literature results, and (h) capacitance retention with cycle number at a current density of 5 A/g of the ASC. (i) Photo graphic image of digital watch operated by one ASC.

synergistic effect of phosphorus and sulfur endows Ni-Co-P-S-2 with superior electrical conductivity and fast kinetics, resulting in elevated electrochemical performance.

To evaluate the practical applications of the Ni-Co-P-S-2 electrode, an asymmetric supercapacitor (ASC) device was assembled (Fig. 4a). Ni-Co-P-S-2 electrode, activated carbon (AC), and cellulose paper were used as the positive electrode, negative electrode, and separator, respectively (denoted as Ni-Co-P-S-2//AC). The CV curves of the Ni-Co-P-S-2//AC ASC device at different voltage windows were recorded at 50 mV/s to optimize the operating voltage window. As displayed in Fig. 4b, stable electrochemical behavior can be maintained in the range of 0–1.6 V. Fig. 4c depicts the CV curves of the ASC device at scan rates from 5 mV/s to 400 mV/s. A pair of hump peak was observed, indicating the existence of pseudo-capacitance in the charge/discharge process. The shape of the CV curves can be maintained with the rising of scan rate, suggesting the excellent rate capability of the ASC. From GCD curves (Fig. 4d), the device showcases a comparative low internal resistance drop, which was caused by the reduced electron/ion diffusion pathway. Encouragingly, the ASC device exhibited excellent capacitances of 110.9, 106.9, 100.7, 93.7, 83.1, 77.8, 70.0 and 62.0 F/g at 1, 2, 3, 5, 10, 15, 20 and 30 A/g, respectively (Fig. 4e). The Nyquist plot (Fig. 4f) displays the charge-transfer resistance value is 0.74 Ω, indicating a low intrinsic resistance of the ASC device.

Fig. 4g shows the Ragone plots of the energy and power density of the ASC device. The ASC showcases a high energy density of 39.11 Wh/kg at a power density of 789 W/kg. Noteworthily, the energy density of the ASC is superior to those of devices based on nickel/cobalt phosphides and sulfides composites previously reported in literatures, such as $NiCo_2S_4$/PRGO//AC (27.5 Wh/kg at 446.5 W/kg) [35], $NiCo_2S_4$//AC (28.3 Wh/kg at 245 W/kg) [36], Ni-Co sulfide NWAs (25 Wh/kg at 3570 W/kg) [37], Ni_8-Co_1-P//AC (22.8 Wh/kg at 4320 W/kg) [38] and $Ni_xCo_{1-x}P$//AC (31.52 Wh/kg at 700 W/kg) [39]. The Ni-Co-P-S-2//AC ASC also displays long-term cycling stability, which was determined by the GCD curves at a high current density of 5 A/g (Fig. 4h). Impressively, 91.87% of the initial capacitance can be maintained after 10,000 cycles, manifesting its excellent stability. Besides, a digital watch can be operated by an ASC device, proving the potential practical use of the Ni-Co-P-S-2//AC ASC device (Fig. 4i).

In summary, interconnected nanowalls-like Ni-Co-P-S nanosheets were successfully prepared *via* a simple one-step electrodeposition procedure. Due to the synergistic effect of multi-component, enriched redox active sites and shortened ion diffusion path, the as-prepared Ni-Co-P-S delivered an ultrahigh specific capacitance of 2744 F/g at 4 A/g, that is superior than those of Ni-Co-S and Ni-Co-P counterparts. In addition, the Ni-Co-P-S-2//AC full supercapacitor device exhibits a potential window of 1.6 V and a superior energy density of 39.4 Wh/kg at a power density of 797.5 W/kg. In addition, the ASC exhibits high capacitance retention of 91.87% after 10,000 cycles, demonstrating a superb cycle life. Accordingly, this work offers a simple approach to metal phospho-sulfide composites for energy conversion/storage.

Declaration of competing interest

The authors report no declarations of interest.

Acknowledgments

This work is financially supported by the National Natural Science Foundation of China (Nos. 52073137, 21704038, 51763018), the NSFC-DFG Joint Research Project (No. 51761135114), the Natural Science Foundation of Jiangxi Province (Nos. 20192BCB23001, 20202ZDB01009).

Appendix A. Supplementary data

Supplementary material related to this article can be found, in the online version, at doi:https://doi.org/10.1016/j.cclet.2021.02.034.

References

[1] Y.H. He, S.W. Liu, C. Priest, Q, et al., Chem. Soc. Rev. 49 (2020) 3484–3524.
[2] W.A. Haider, M. Tahir, L. He, et al., ACS Central Sci. 6 (2020) 1901–1915.
[3] L.F. Zhu, Y.H. Qu, X.Y. Huang, et al., Chem. Commun. 56 (2020) 13201–13204.
[4] X.J. Chen, W. Li, Y.B. Xu, et al., Nano Energy 75 (2020) 104869.
[5] Z.G. Yang, Z.G. Wu, W.B. Hua, et al., Adv. Sci. (2020) 1903279.
[6] J. Huang, J.C. Wei, Y.B. Xiao, et al., ACS Nano 12 (2018) 3030–3041.
[7] W.Y. Chen, X.M. Zhang, Y.Q. Peng, et al., J. Power Sources 438 (2019) 227004.
[8] Y.Z. Li, R. Cao, L.B. Li, et al., Small 16 (2020) 1906735.
[9] H.J. Xu, J. Cao, C.F. Shan, et al., Angew. Chem. Int. Ed. 57 (2018) 8654–8658.
[10] T.Y. Liu, P. Diao, Z. Lin, et al., Nano Energy 74 (2020) 104787.
[11] Y.M. Li, J. Liu, X.Y. Li, et al., ACS Appl. Mater. Interfaces 11 (2019) 27170–27177.
[12] Y.P. Liu, Y.X. Wen, Y.N. Zhang, et al., Sci. China Mater. 63 (2020) 1216–1226.
[13] L.F. Shen, J. Wang, G.Y. Xu, et al., Adv. Energy Mater. 5 (2015) 1400977.
[14] X.Y. Yu, X.W. Lou, Adv. Energy Mater. 8 (2018) 1701592.
[15] P.B. Geng, S.S. Zheng, H. Tang, et al., Adv. Energy Mater. 8 (2018) 1703259.
[16] J. Balamurugan, C. Li, S.G. Peera, et al., Nanoscale 9 (2017) 13747–13759.
[17] Z.Y. Peng, L.Y. Gong, J. Huang, et al., Carbon 153 (2019) 531–538.
[18] Y. Wang, J. Huang, Y.B. Xiao, et al., Carbon 147 (2019) 146–153.
[19] Y.B. Xiao, J. Huang, Y.Z. Xu, et al., J. Mater. Chem. A 6 (2018) 9161–9171.
[20] M. Guo, J. Balamurugan, T.D. Thanh, et al., J. Mater. Chem. A 4 (2016) 17560–17571.
[21] C.Y. Zhang, X.Y. Cai, Y. Qian, et al., Adv. Sci. 5 (2018) 1700375.
[22] W.D. He, C.G. Wang, H.Q. Li, et al., Adv. Energy Mater. 7 (2017) 1700983.
[23] W.H. Luo, G.F. Zhang, Y.X. Cui, et al., J. Mater. Chem. A 5 (2017) 11278–11285.
[24] W. Lu, J.L. Shen, P. Zhang, et al., Angew. Chem. Int. Ed. 58 (2019) 15441–15447.
[25] B. Jiang, X.H. Ban, Q. Wang, et al., J. Mater. Chem. A 7 (2019) 24374–24388.
[26] X.Y. Lei, S.C. Ge, Y.H. Tan, et al., J. Mater. Chem. A 7 (2019) 24908–24918.
[27] W. Chen, C. Xia, H.N. Alshareef, ACS Nano 8 (2014) 9531–9541.
[28] H.Z. Lv, Q. Pan, Y. Song, et al., Nano-Micro Lett. 12 (2020) 118.
[29] T. Zhang, K.N. Yang, C. Wang, et al., Adv. Energy Mater. 8 (2018) 1801690.
[30] K.Y. Zhang, Y.H. Wei, J. Huang, et al., Sci. China Mater. 63 (2020) 1898–1909.
[31] S.Y. Li, W. He, B. Liu, et al., Energy Storage Mater. 25 (2019) 636–643.
[32] J. Huang, Y.S. Xiong, Z.Y. Peng, et al., ACS Nano 14 (2020) 14201–14211.
[33] K. Raju, H. Han, D.B. Velusamy, et al., ACS Energy Lett. (2019) 23–30.
[34] H.H. Fan, B.W. Qin, Z.W. Wang, et al., Sci. China Mater. 63 (2020) 505–515.
[35] Y.W. Zheng, X.X. Wang, W. Zhao, et al., Chem. Eng. J. 333 (2018) 603–612.
[36] Y.R. Zhu, Z.B. Wu, M.J. Jing, et al., J. Power Sources 273 (2015) 584–590.
[37] Y.H. Li, L.J. Cao, L. Qiao, et al., J. Mater. Chem. A 2 (2014) 6540–6548.
[38] R. Ding, X.D. Li, W. Shi, et al., Chem. Eng. J. 320 (2017) 376–388.
[39] Y.Q. Xu, S.J. Hou, G. Yang, et al., Electrochim. Acta 285 (2018) 192–201.